ANL-ART-204

Sample problems for Section III, Division 5 design by inelastic analysis of Grade 91 components

Applied Materials Division

ANL-ART-204

Sample problems for Section III, Division 5 design by inelastic analysis of Grade 91 components

Applied Materials Division
Argonne National Laboratory

September 2020

Prepared by

Guosheng Ye
Mark C. Messner
T.-L. Sham

ABSTRACT

This report works through two sample design analyses of representative Grade 91 components using the ASME Boiler & Pressure Vessel Code Section III, Division 5, Appendix HBB-T rules for the strain and deformation and creep-fatigue design criteria using a design by inelastic analysis approach. The component geometries and loadings were selected to span a wide variety of potential applications. The sample components are an endplate geometry, which is fairly representative of typical pressure vessel construction, and a core block, representing a critical component in a heat pipe microreactor, which has a complicated geometry and complex thermal stress history. These sample problems serve several functions. First, they are complete worked examples of how to apply the current design by inelastic analysis rules. Second, they serve as test cases to evaluate the current rules and provide feedback on how they could be optimized to deal with complicated component geometries or to be better automated in modern finite element analysis software. Finally, the analysis here uses an inelastic constitutive model for Grade 91 developed by Argonne National Laboratory and proposed for inclusion in the ASME Boiler & Pressure Vessel Code Section III, Division 5 rules as a reference constitutive model. Using this constitutive model in the sample problem analyses tests the model in the context of the ASME Code rules. The final conclusions of this report are that the material model and the current Code rules are satisfactory, but that the Code rules could be optimized to simplify automation and reduce over conservatism. Future work should address the specific optimization topics discussed in this report.

TABLE OF CONTENTS

LIST OF FIGURES

LIST OF TABLES

1 Introduction

1.1 Overview of this report

Section III, Division 5 [1] Appendix HBB-T of the ASME Boiler and Pressure Vessel Code provides design by inelastic analysis criteria for evaluating the strain and creep-fatigue damage criteria for Class A components. Historically, design by inelastic analysis has been seen as less over-conservative, producing more efficient structural designs than the design by elastic analysis rules. For example, in the Clinch River Breeder Reactor Project (CRBRP), design by elastic analysis was used to design the majority of the plant systems, whereas design by inelastic analysis was only applied to the most challenging parts of the structural components where the elastic rules could not produce a feasible design [4]. Part of the difficulty in the CRBRP was that the computational resources available at the time could not apply the design by inelastic analysis rules to large components. Modern computing resources are, of course, substantially larger, potentially allowing the application of the efficient design by inelastic analysis to a wider array of components.

This report provides sample design by inelastic analysis examples, following the Appendix HBB-T rules, for two different Grade 91 component designs: a core block geometry, for example as part of a heat-pipe microreactor, and an endplate, i.e. a connection between a larger diameter cylinder and a smaller diameter cylinder with a welded join in between. These components are complementary: the endplate is a typical feature of standard pressure vessel construction falling within the range of structures considered during the development of the HBB-T rules, whereas the core block is a more unique geometry likely not considered during the initial development of the rules.

The purpose of these analyses is to both to provide worked sample problems applying the design by inelastic rules to Grade 91 components and also to assess the current rules, particularly for use with complicated geometries like the core block. This report then provides a detailed description of the analysis of each component but also an assessment of the current design by inelastic analysis rules, given in Chapter 4. The overall conclusion is that the current rules are adequate and workable, but optimizations are possible to simplify the automation of the design process in modern finite element frameworks and to reduce over-conservatism.

1.2 Background

When high temperature components are designed, their functionality and structural integrity during service under creep deformation needs to be maintained. Evaluation of damage due to creep and fatigue is also required in order to check for local material failure during service. The ASME Boiler and Pressure Vessel Code (BPVC) Section III, Division 5, Appendix HBB-T provides design by elastic analysis and design by inelastic analysis rules covering these criteria for high temperature reactor components [1]. Compared with the inelastic rules, elastic analysis requires much less computational resources and simpler material models, but it also tends to produce overly conservative results and higher cost components. Stress linearization location selection and stress classification in the elastic analysis process are always a challenge, particularly for new types of component designs versus conventional cylindrical pressure vessels. For new component types, analysts' previous experience will not provide guidance for stress linearization path location and

ambiguities exist on issues such as whether a thermal load should be partially regarded as primary load, due to possible severe elastic follow-up.

In recent decades, progress in computer hardware, software, computation algorithms provides opportunities for design by inelastic analysis. Development in material testing and analysis techniques has produced accurate constitutive models describing material deformation in elevated temperature conditions. In the following chapters, we will present the inelastic analysis of the endplate and core block geometries on a computer cluster with 40 CPU cores and 500 GB memory. A Grade 91 constitutive model developed by ANL and proposed forincorporation in Section III, Division 5 Appendix HBB-Z rules was used for the analysis [2]. The FEA software was ANSYS Mechanical version 2019 R2.

1.3 Scope of the analysis

Two different component geometries are analyzed in this report. The first is a representative core block geometry of a heat pipe microreactor with the characteristic fuel rod and heat pipe holes. The second is a component where two cylinders with different sizes are connected through a fillet weld at the joint between the smaller size cylinder and an endplate, and a butt weld joint between the endplate and the larger size cylinder. This component will be referred to as an “endplate” in short. This report demonstrates how to apply the inelastic analysis approach to these two components and how to check their compliance with the Appendix HBB-T design by inelastic analysis rules for strain limits and creep-fatigue damage.

2 Analysis

2.1 Acceptance criteria

Appendix HBB-T in [1] specifies two sets of acceptance criteria for inelastic analysis: strain and deformation limits and creep-fatigue damage.

2.1.1 Deformation and strain limits

In Paragraph HBB-T-1310 *Limits for inelastic strains*, it specifies that the maximum accumulated inelastic strain shall not exceed:

(a) Strains averaged through the thickness, 1%
(b) Strains at the surface, due to an equivalent linear distribution of strain through the thickness, 2%.
(c) Local strains at any point, 5%.

In the above, these limits apply to the maximum positive value of the three principal strains. The strains in (a) and (b) are first averaged and linearized, respectively, for each strain component before combined to determine the principal strains for comparison to the respective limit in (a) and (b). The principal strains from the strains in (c) are based on the computed strains at the point of interest.

2.1.2 Creep-fatigue interaction damage

For a design to be acceptable, the damage due to creep and fatigue during service should satisfy

$$\sum_{j=1}^{p}\left(\frac{n}{N_d}\right)_j + \sum_{k=1}^{q}\left(\frac{\Delta t}{T_d}\right)_k \le D \tag{1}$$

Where $(n)_j$ is the number of type j cycle; $(N_d)_j$ is the number of allowable type j cycle, determined from the HBB-T fatigue curves (implemented here in the hbbdata software package [3]), the design fatigue range for Grade 91, corresponding to the maximum metal temperature occurring during the cycle; p is the number of cycle types, q is the number of time intervals at specified temperatures during whole service life; $(\Delta t)_k$ is the duration of the time interval k, $(T_d)_k$ is the allowable time duration for the time interval k at a given stress and the maximum temperature; D is the total allowable creep-fatigue damage, from Figure HBB-T-1420-2 in the Code.

The procedures for calculation $(N_d)_j$ and $(T_d)_k$ are described below, summarizing HBB-T-1430 [1].

2.2 Methodology

2.2.1 Grade 91 material model

The Gr.91 material model adopted for the inelastic analysis in this report was developed by Messner et al. [2], the model includes material kinematic/isotropic hardening, tension/compression asymmetry, and unifies plastic deformation and creep together through Kocks-Mecking diagram

approach. The parameters in the model were based on the material average response from different batches of experimental data [2].

2.2.2 Time increment determination

The service level loadings were specified in the design specifications. For inelastic analysis, as the material model is inelastic, i.e., history/path dependent, the smaller the time increment the more accurate the analysis results. However, more time increments leads to longer FEA analysis and post-processing times. For the two cases considered in this report, the material properties are temperature dependent. In order to capture the possible thermal stress peaks during temperature ramping periods, the maximum temperature changes were restricted to be less than 10^{o} C per time increment. The structural deformation and heat conduction are assumed to be decoupled in the ANSYS FEA. Therefore, the thermal model was run first and the temperature fields in the result data frames were input into the structural model.

2.2.3 Strain linearization

Except for the local maximum principal inelastic strain criteria $\varepsilon_{p,total}$, in order to fulfill the strain requirement described in Section 2.1.1, the inelastic strains accumulated had to be linearized based on Equation 1 and 3 below.

$$\varepsilon_{ij,p,m} = \frac{1}{t}\int_0^t \varepsilon_{ij,p}\,dx \qquad i,j = 1,2,3,\ t \text{ is the wall thickness} \tag{1}$$

Based on those membrane components $\varepsilon_{ij,p,m}$, three principal inelastic membrane strains $\varepsilon_{1,p,m}$, $\varepsilon_{2,p,m}$, $\varepsilon_{3,p,m}$ were obtained and maximum principal inelastic membrane strain was defined as

$$\varepsilon_{p,m} = \max\left(\varepsilon_{1,p,m}, \varepsilon_{2,p,m}, \varepsilon_{3,p,m}\right) \tag{2}$$

Where $\varepsilon_{ij,p,m}$: the inelastic strain membrane component;

$\varepsilon_{ij,p}$: the inelastic strain component;

$\varepsilon_{p,m}$: the maximum principal membrane inelastic strain;

$\varepsilon_{i,p,m}$: the principal inelastic membrane strains;

$\varepsilon_{ij,p,b}$, the bending part of the inelastic strain component is calculated as

$$\varepsilon_{ij,p,b} = \frac{6}{t^2}\int_0^t \varepsilon_{ij,p}\left(\frac{t}{2} - x\right)dx \tag{3}$$

To satisfy Item (a) mentioned in Section 2.1.1, the positive $\varepsilon_{p,m}$ values should be applied. In order to get the surface strain for Item (b), the linearized strain components were calculated then based on the six new strain components $\varepsilon_{ij,p,m+b}$, the definition applied to get the maximum principal strain $\varepsilon_{p,m+b}$.

2.2.4 Strain and deformation limit calculation procedure

The inelastic analysis results contained data frames at different times through several repeated load cycles. Analyzing each data frame was impractical and the time spots for which the data frames were extracted for strain and deformation limit checks had to be selected manually. For the two cases in the report, they were determined to be the data frames at the end of each load cycle. The reason was that during each load cycle, the material underwent a process of loading/holding/unloading process, and holding stage was the period when the inelastic strain kept increasing and the changes during loading and unloading were negligible. Figure 2.1 demonstrates the accumulated equivalent inelastic strain during load cycles in the model and during loading/unloading, the curve remains flat. To check local maximum principal inelastic strain ($\varepsilon_{p,total}$) limit, i.e., 5% for the base metal and 2.5% for the weld, the steps were as follows:

Step 1: Observe the maximum principal inelastic strain ($\varepsilon_{p,total}$) contour plot at the end of each load cycle, to ensure the maximum $\varepsilon_{p,total}$ location was always at the same location with the same direction, if not, continue to run more load cycles.
Step 2: Probe the $\varepsilon_{p,total}$ values at the end of each load cycle for the model. If the data showed that the values changed from cycle to cycle with decreasing magnitude or no change, continue. If neither occurs continue to run more load cycles.
Step 3: Use the $\varepsilon_{p,total}$ value at the end of the last load cycle and the its magnitude difference from that of the cycle before it to predict the its value at the end of the service life, i.e., if 5 total load cycles were run in FEA, the $\varepsilon_{p,total}$ value at the end of the 5th cycle and its change during the 5th cycle were applied to predict the $\varepsilon_{p,total}$ values at the required 30 load cycles.
Step 4: If the maximum $\varepsilon_{p,total}$ value in the model did not occur at the weld, the above Step 1 to Step 2 had to be repeated for the maximum value at the weld.

The inelastic membrane strain limit (1% for base metal, 0.5% for the weld) and surface strain limit (2% for the base metal 1% for the weld) were examined by the following steps:

Step 1: By observing the local maximum principal inelastic total strain $\varepsilon_{p,total}$ contour plots at the end of each load cycle, the strain linearization path (SLP) was decided.
Step 2: For the data frames at the end of each load cycle, the six inelastic strain components $\varepsilon_{ij,p}$, $i,j = 1,2,3$ along the SLP and got membrane part $\varepsilon_{ij,p,m}$, and bending part $\varepsilon_{ij,p,b}$, for each strain component through linearization procedure described in Section 2.2.3.
Step 3: Based on the $\varepsilon_{ij,p,m}$ values, compute the maximum inelastic principal membrane strain $\varepsilon_{p,m}$; based on $\varepsilon_{ij,p,m}$ and $\varepsilon_{ij,p,b}$, compute the maximum inelastic principal surface strains $\varepsilon_{p,m+b}$ (summed up for each component first, for both inside wall and outside wall).
Step 4: Repeat Step 2 and Step 3 for the data frame at the end of each load cycle.
Step 5: The maximum inelastic principal membrane strains $\varepsilon_{p,m}$ and surface strains $\varepsilon_{p,m+b}$ obtained by following above steps should show decreasing or no change from cycle to cycle, if the changing magnitude kept increasing, more load cycles were needed and repeated Step 2 and Step 3.
Step 6: Used the $\varepsilon_{p,m}$ value at the end of the last load cycle computed along with the difference with the cycle before it, to predict the its value at the end of the service life, i.e., total 5 load cycles were run in FEA, the $\varepsilon_{p,m}$ value at the end of the 5th cycle and its

changes during the 5th cycle were applied to predict the $\varepsilon_{p,m}$ values at the required 30 load cycles. The same was done with inside wall and outside wall principal surface strains $\varepsilon_{p,m+b}$.

Step 7: If the critical SLP did not occur at the weld, engineering judgment would suggest Step 1 to Step 6 to be repeated for the maximum value for the welds, even though that value was not the maximum for the whole model because the weld allowable strain limit is lower than that for base metal.

Figure 2.2 illustrates the process of assessing the inelastic strain distribution against the three strain limit criteria.

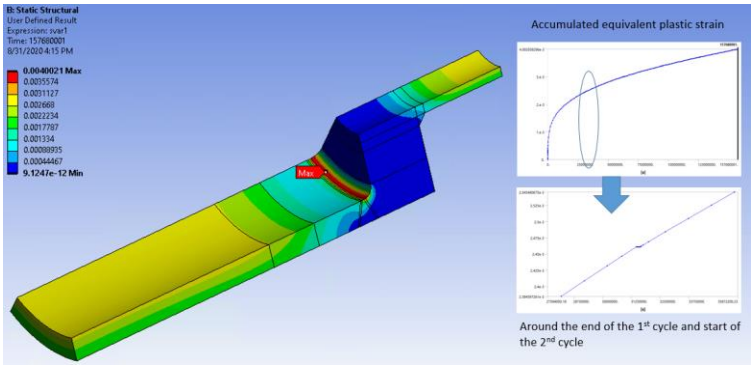

Figure 2.1. Accumulated equivalent inelastic strain at the critical deformation location (near the weld) in the end-plate model.

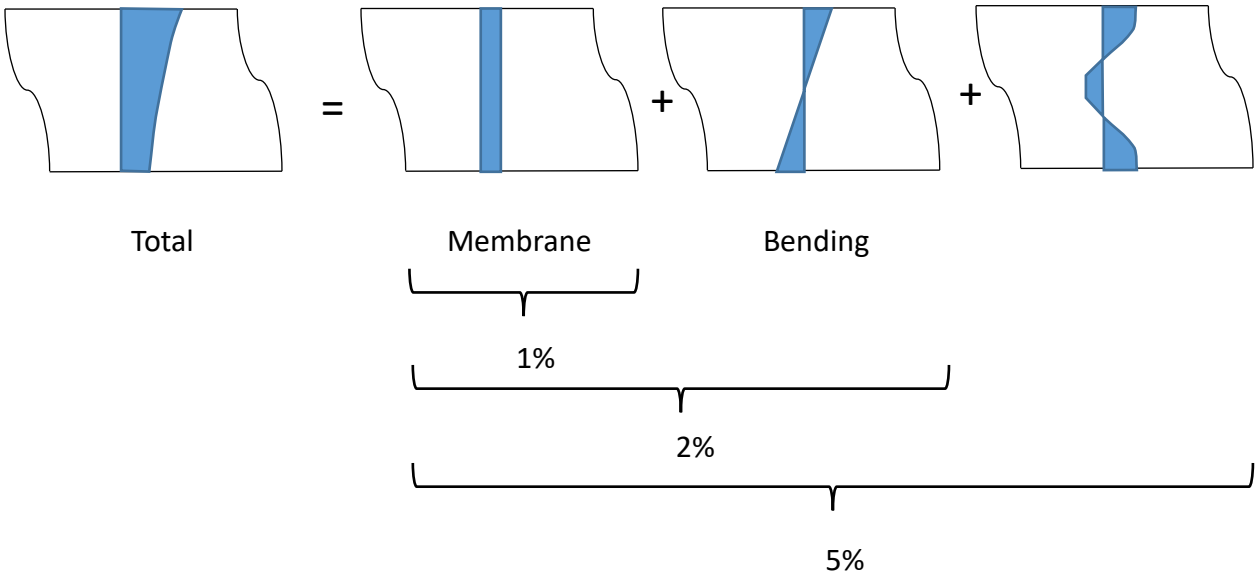

Figure 2.2. Illustration of how the inelastic strain is decomposed and compared to the strain limits. The scalar values are the maximum principal strain for the corresponding distribution. The strain limits only consider residual inelastic strain. The allowable strains for welds are half of those shown in the figure.

2.2.5 Creep-fatigue calculation procedure

Paragraph HBB-T-1420 of [1] provides guidance on creep-fatigue damage calculation using inelastic analysis, the following paragraphs provide more details of the calculation method applied here.

2.2.5.1 Fatigue damage

The critical part of the calculation is the maximum strain range determination. In inelastic analysis, the FEA results provided total strain (elastic + inelastic) component data frames for each time step, through permutation of those data frames, the maximum strain range was obtained. The strain range $\Delta\varepsilon_{equiv,i}$ between strain data frames from two time steps *i* and *o* was calculated by Equation (4) below from Paragraph HBB-T-1413 [1]:

$$\Delta\varepsilon_{equiv,i} = \frac{\sqrt{2}}{3}\Big[\left(\Delta\varepsilon_{xi} - \Delta\varepsilon_{yi}\right)^2 + \left(\Delta\varepsilon_{yi} - \Delta\varepsilon_{zi}\right)^2 + (\Delta\varepsilon_{xi} - \Delta\varepsilon_{zi})^2 + \frac{3}{2}\left(\Delta\gamma_{xyi}{}^2 + \Delta\gamma_{yzi}{}^2 + \Delta\gamma_{xzi}{}^2\right)\Big]^{\frac{1}{2}} \quad (4)$$

Where $\Delta\varepsilon_{xi} = \varepsilon_{xi} - \varepsilon_{xo}$;
$\Delta\varepsilon_{yi} = \varepsilon_{yi} - \varepsilon_{yo}$;
$\Delta\varepsilon_{zi} = \varepsilon_{zi} - \varepsilon_{zo}$;
$\Delta\gamma_{xyi} = \gamma_{xyi} - \gamma_{xyo}$;
$\Delta\gamma_{yzi} = \gamma_{yzi} - \gamma_{yzo}$;
$\Delta\gamma_{xzi} = \gamma_{xzi} - \gamma_{xzo}$;
$\varepsilon_{xi}, \varepsilon_{yi}, \varepsilon_{zi}, \gamma_{xyi}, \gamma_{yzi}, \gamma_{xzi}$ are the six strain components for time step *i* and
$\varepsilon_{xo}, \varepsilon_{yo}, \varepsilon_{zo}, \gamma_{xyo}, \gamma_{yzo}, \gamma_{xzo}$ are for time step *o*.

This algorithm was implemented in an ANSYS ACT plugin developed at Argonne. The plugin performs the post-processing of the data frames and provides a contour plot of maximum strain range at each location for each load cycle across the entire model. The highest maximum strain range in the base metal and that for the weld had to be selected separately for fatigue damage calculation as the allowable number of cycles for the weld are only half of that for the base metal.

In the inelastic analysis presented here, the FEA only ran 5 load cycles, the maximum strain ranges were obtained for each cycle, and the data had to be extrapolated for a conservative prediction of allowable number cycles for fatigue damage calculation. Fatigue damage was the ratio of expected number of cycles to allowable number of cycles N_d, which could be obtained from related HBB-DATA package functions [3].

2.2.5.2 Creep damage

Section HBB-T-1420 in Appendix HBB-T of [1] provides an equation for creep damage calculation:

$$creep\ damage = \int_0^t \frac{dt}{T_d} \quad (5)$$

where *t* is the time, *dt* is the time increment and T_d is the rupture life based on the stress and temperature during that time increment. The equation was combined into ANSYS USERMAT subroutine and creep damage was output as a state variable.

To calculate T_d, effective stress σ_e was obtained from [1] as,

$$\sigma_e = \overline{\sigma} exp\left[C\left(\frac{J_1}{S_s} - 1\right)\right] \tag{6}$$

Where $J_1 = \sigma_1 + \sigma_2 + \sigma_3$;

$S_s = ({\sigma_1}^2 + {\sigma_2}^2 + {\sigma_3}^2)^{\frac{1}{2}}$;

$\overline{\sigma} = \frac{1}{\sqrt{2}}[(\sigma_1 - \sigma_2)^2 + (\sigma_2 - \sigma_3)^2 + (\sigma_3 - \sigma_1)^2]^{\frac{1}{2}}$

$\sigma_1, \sigma_2, \sigma_3$ are the three principal stresses, C is a constant for Gr.91 defined as follows:

(1) If $J_1/Ss >= 1.0$, $C = 0.16$;

(2) If $J_1/Ss < 1.0$, $C = 0$.

A design factor *K'* is introduced in [1] and the value of σ_e/K' is substituted into the creep rupture correlation to obtain the rupture life. The *K'* factor is specified in [1] as 0.67 for inelastic analysis. It is noted that a value of 0.9 is assigned to the *K'* factor when the stresses are determined from the elastic analysis approach. In the following, a *K'* value of 0.9 was also applied to σ_e from the inelastic analysis results to assess the effect of the difference in margin between these two design factors. To get the creep-rupture life as a function of stress and temperature, the data from HBB-DATA package were fit into an equation through regression in the temperature range 390° C and 650° C, and stress range from 1MPa to 400 MPa. Equation 7 below shows the relationship between rupture life, stress and temperature, based on the Code minimum stress-to-rupture table, with an R^2 value of 0.953.

$$ln(t_r) = \frac{7.971E4 - 65.8106\sigma + 0.0308\sigma^2}{T} - 75.5102 \tag{7}$$

Where t_r is the creep-rupture life in hours, σ is the modified effective stress σ_e/K' in MPa and *T* is the temperature in kelvin.

For the creep damage at the welds, the effective creep stress was first divided by the stress rupture (*R)* factor, given in Table HBB-I-14.10E-1. As the *R* factor is a function of temperature, a function was written in FORTRAN to interpolate for any temperature between 425° C and 650° C, when temperature was less than 425° C or larger than 650° C, *R* values were the same as those at 425° C

or 650^{o} C, respectively. This *R* interpolation function was part of the ANSYS USERMAT subroutine module.

2.2.5.3 Creep-fatigue interaction

Given the individual creep and fatigue damage fractions, the creep-fatigue acceptance criteria is to check to see if the point falls in the envelope given in Figure HBB-T-1420-2.

2.3 Assumptions

This analysis is based on the following assumptions:

1. Materials are isotropic and homogeneous; material response is constant over time, i.e., effects of material degradation over time, are neglected.
2. The material thermo-physical properties and constitutive equations applied in FEA are the same for both the welds and the base metal.
3. Residual stresses are not included at the beginning of the first load cycle.
4. The temperature transients and pressure transients are representative of the component operating conditions.

3 Results

3.1 Analysis input

3.1.1 Geometry and mesh

The core block geometry was generated through ANSYS SpaceClaim® scripting and consists of holes for heat pipe and fuel rods. The geometry of the endplate was from a set of Grade 91 sample problems used in Section VIII ASME Code Committees to assess high temperature design methods [5]. The two geometries and their dimensions are shown in Figure 3.1 below.

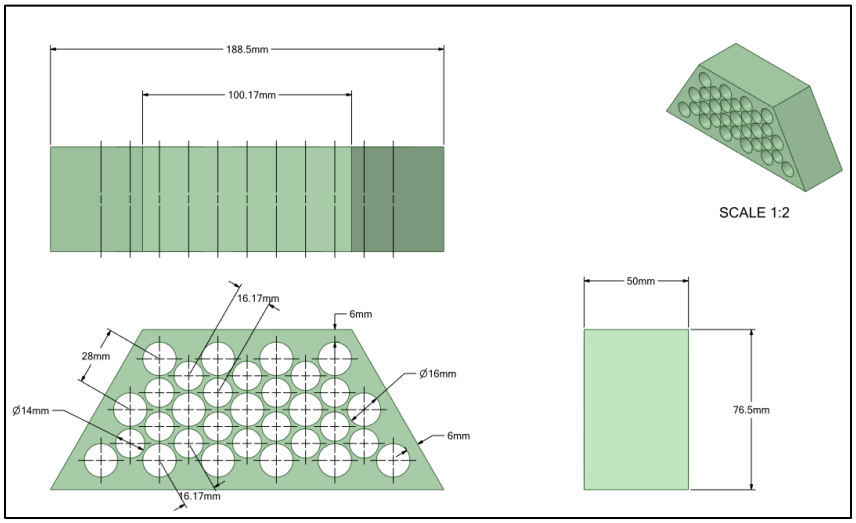

(a)

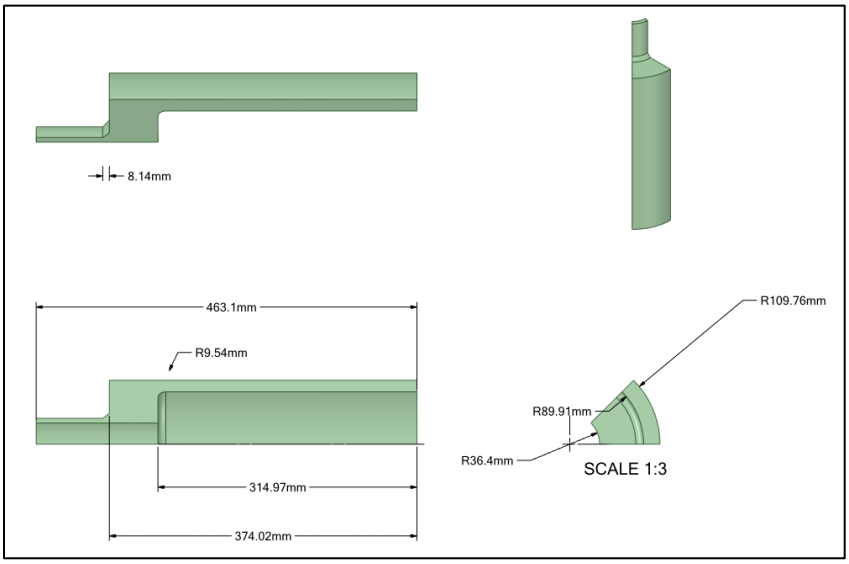

(b)

Figure 3.1. Geometry for the core block problem (a) and the endplate problem (b).

The number of quadratic solid elements in the core block model and the endplate model are 9420 and 32240, respectively. The models with meshes are displayed in Figure 3.2 below.

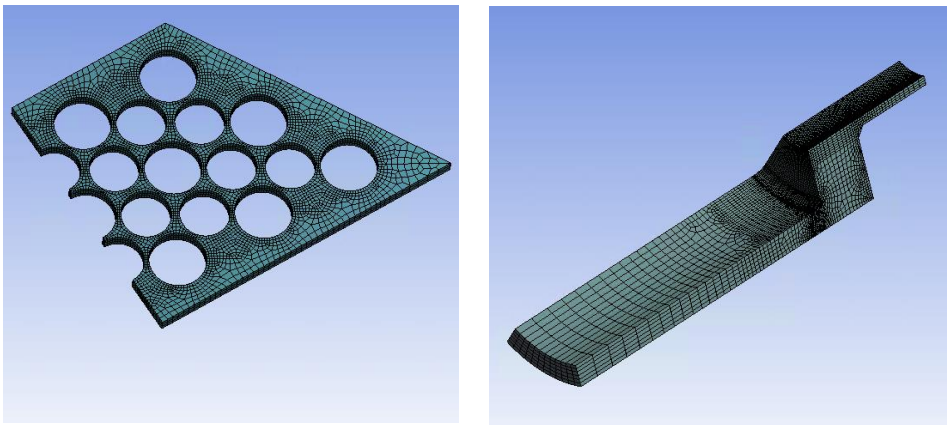

(a) (b)

Figure 3.2. Meshes for the models. (a) core block, (b) endplate.

3.1.2 Material models

Section 2.2.1 describes the Grade 91 material model used in the analysis. Basic thermal properties and the HBB design data were provided by HBBDATA package [3], developed at ANL.

3.1.3 Boundary conditions

3.1.3.1 Core block

3.1.3.1.1 Mechanical loads and boundary conditions

The magnitude of the pressure load was very small and the load was negligible. The mechanical boundary conditions are shown in Figure 3.3 below. The z-displacements of the top/bottom planes was either fixed, as shown in Figure 3.3 (a), or coupled, as shown in Figure 3.3 (b). For the side planes, two of them could only move within their own planes, and the other two planes were free of constraints.

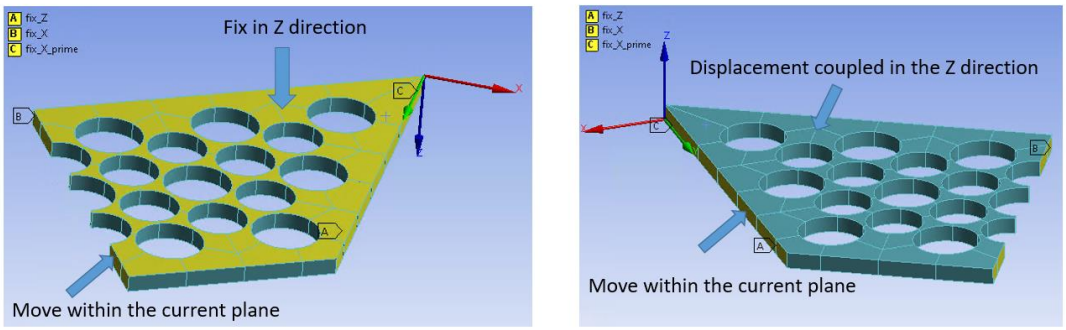

(a) (b)

Figure 3.3. Mechanical boundary conditions for the core block problem.

3.1.3.1.2 Thermal loads and boundary conditions

The initial temperature of the component was 350° C and the initial heat flux at the fuel rod hole walls was 0. During each thermal load cycle, at full load, the fuel rod hole walls were heated with a flux of 25000 W/m^2, and the heat pipe hole walls were held with a constant temperature of 550° C. At the beginning of the load cycle and at the end of the full load holding period, the loads ramped up/down uniformly within 20 hours. The locations for the thermal loads are displayed in Figure 3.4 and the thermal load transients for one cycle are shown in Figure 3.5. There were 5 thermal load cycles in the FEA model and total 360 cycles within the service life.

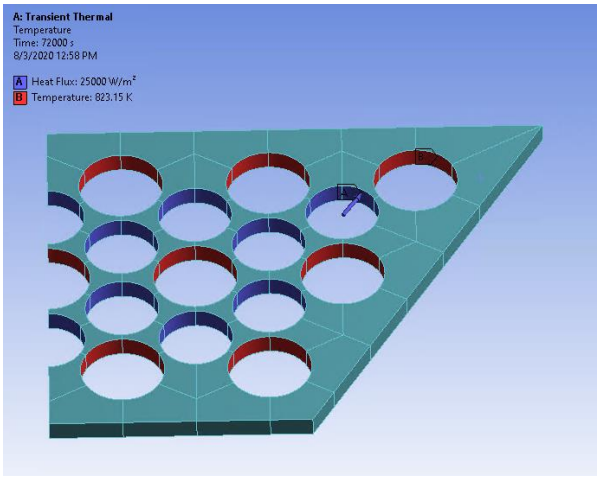

Figure 3.4. Thermal loads in core block FEA model.

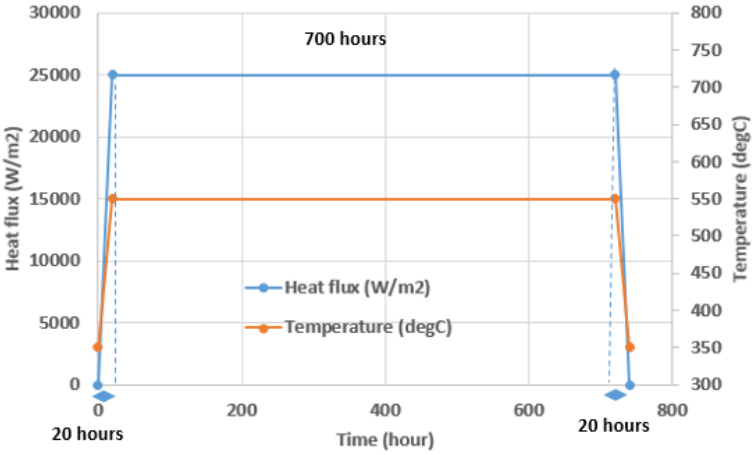

Figure 3.5. Thermal load transients for the core block FEA model.

3.1.3.2 Endplate

3.1.3.2.1 Mechanical loads and boundary conditions

The steady state pressure load was 16.2MPa, which was applied at the internal surface of the model and also introduced as an end load at the smaller diameter cylinder. One pressure cycle involved ramping up from 0 MPa to the full load in a day and keeping the pressure load for 365 days and ramping down to 0 MPa within one day. For the endplates model, the FEA ran 5 pressure load cycles (30 cycles for whole service life). For mechanical boundary conditions, the larger diameter cylinder end was fixed in the axial direction and the smaller cylinder end was coupled in the same direction; the two side planes could only move within their own planes. The mechanical load and boundary conditions for the endplate model are shown in Figure 3.6 below.

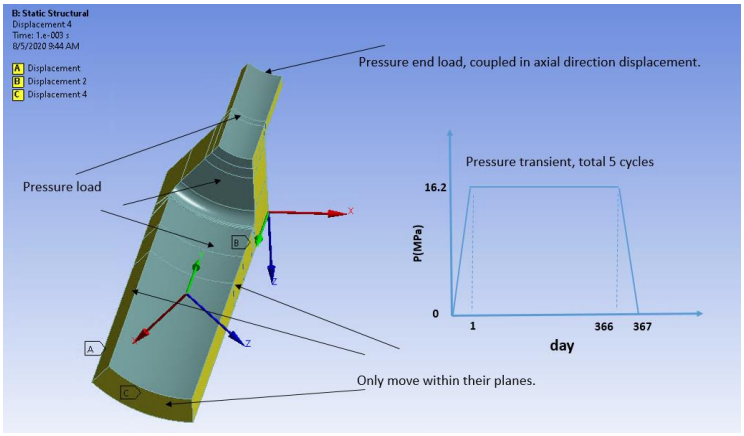

Figure 3.6. Mechanical boundary conditions for the endplate problem.

3.1.3.2.2 Thermal loads and boundary conditions

The endplate internal surface, where the internal pressure load was applied, also underwent thermal load, the convective heat transfer coefficient there was 2000 $W/(m^2.K)$ and the fluid bulk temperature transient are displayed in Figure 3.7 below. There were 5 heat load cycles in the FEA for

endplate model and 30 cycles for the whole service life. Except for the internal surface where the convective thermal load is applied, all other surfaces were thermally insulated.

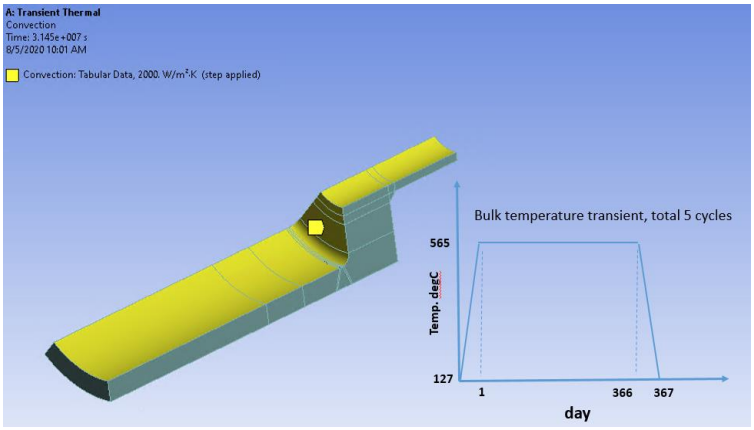

Figure 3.7. Thermal loads in the endplate model.

3.2 Design calculation results

The inelastic analysis results are divided into two parts, one part for strain and deformation limit check and one part for creep-fatigue damage check. The results for the core block model and endplate models are presented separately inside each section.

3.2.1 Strain and deformation limits

3.2.1.1 Core block

The maximum principal inelastic strain $\varepsilon_{p,total}$ over the hold period during the 1st cycle are shown in the contour plots in Figure 3.8 below. This figure illustrates that the highest values occurs in the webs between the fuel rod holes and are less than $5\text{x}10^{-6}$. The maximum values in the plots through the five load cycles are shown in Figure 3.9. The maximum principal plastic strain continues decreasing from cycle to cycle, and is much less than 1%, 2% and 5% strain limits. The data demonstrates the structure shakes down and does not accumulate significant inelastic strain.

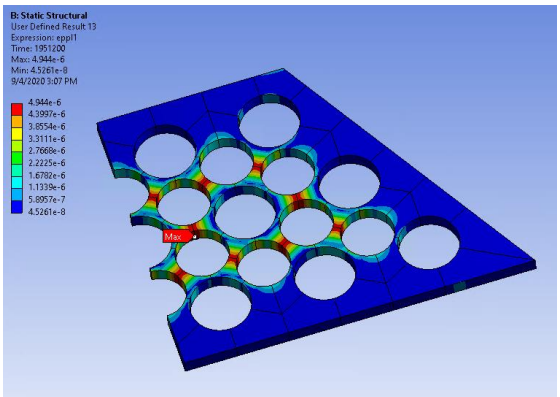

Figure 3.8. Maximum principal inelastic strain during the first hold.

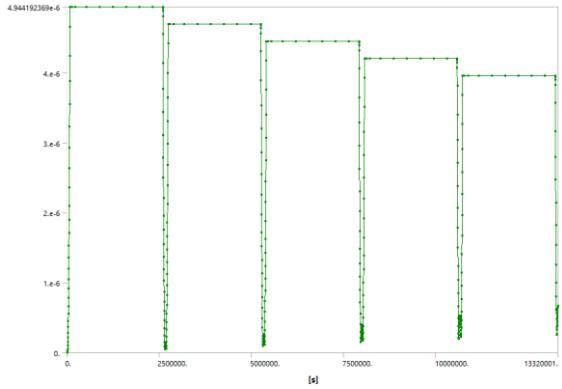

Figure 3.9. The maximum values for each maximum principle inelastic strain during the 5 load cycles.

3.2.1.2 Endplate

3.2.1.2.1 Local maximum principal inelastic strain limit check

Figure 3.10 (a) to (e) below displays the maximum principal inealstic strain $\varepsilon_{p,total}$ contour plots and (f) illustrates how the maximum values change through the 5 load cycles. Figure 3.11(a) to (d) below show change in strain between two consequent load cycles. The two figures show that during the five load cycles, $\varepsilon_{p,total}$ keeps increasing, but with decreasing magnitudes. Table 3.1 shows the $\varepsilon_{p,total}$ values at the end of each load cycles and at the location of the maximum value in the whole model. The maximum $\varepsilon_{p,total}$ value at the end of the 5th cycle is 3.4109E-3 and the $\varepsilon_{p,total}$ increase in magnitude during the 5th cycle is 2.472E-4. A conservative estimation of $\varepsilon_{p,total}$ at the end of service life (30 cycle) is 9.59E-3, which is smaller than the 2.5% strain requirement for the weld, as the location is close to the welded joint.

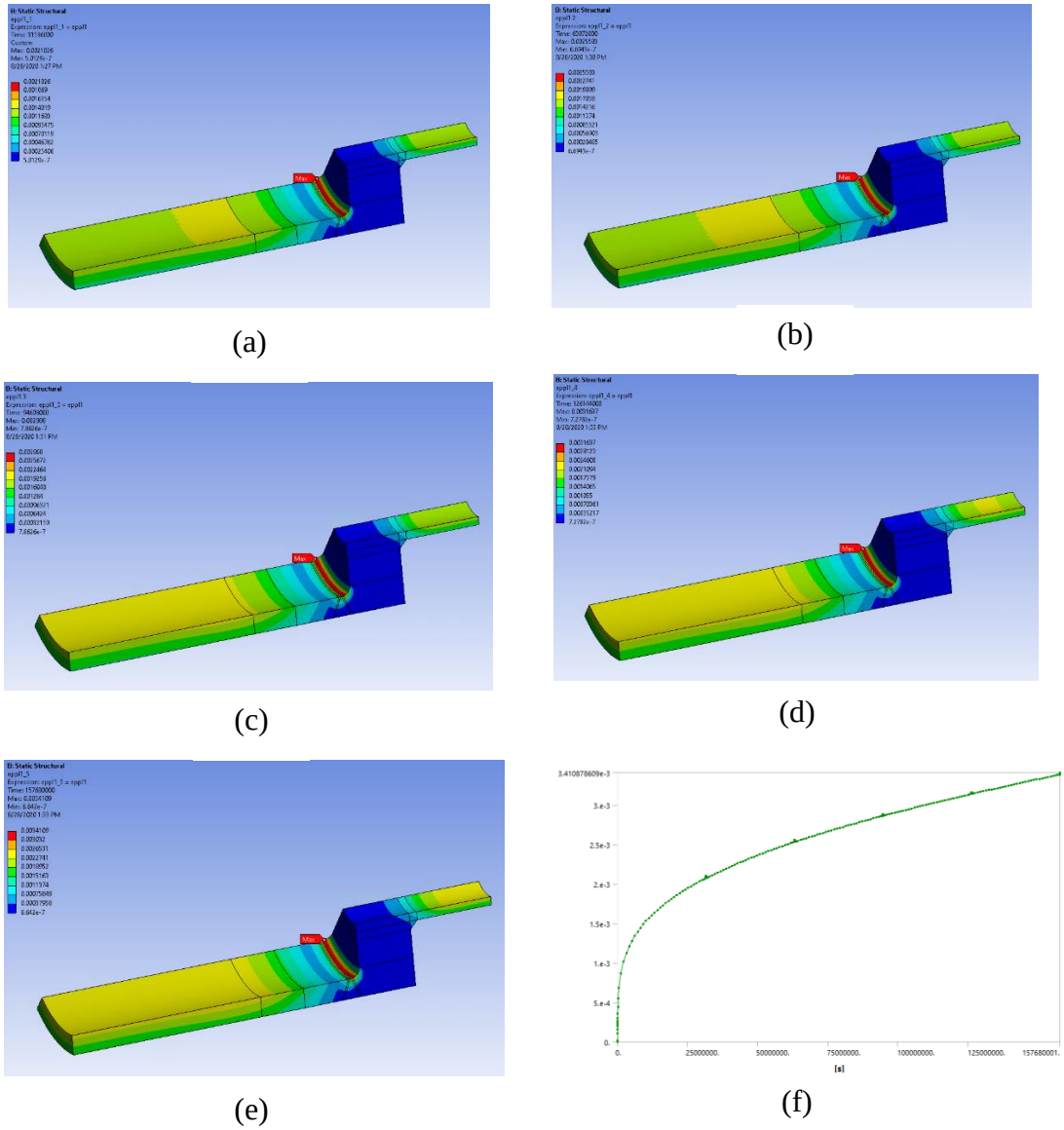

Figure 3.10. Maximum principal inelastic strain at the end of each load cycle for the endplate model (a) 1st cycle. (b) 2nd cycle. (c) 3rd cycle. (d) 4th cycle. (e) 5th cycle. (f) maximum values through 5 load cycles.

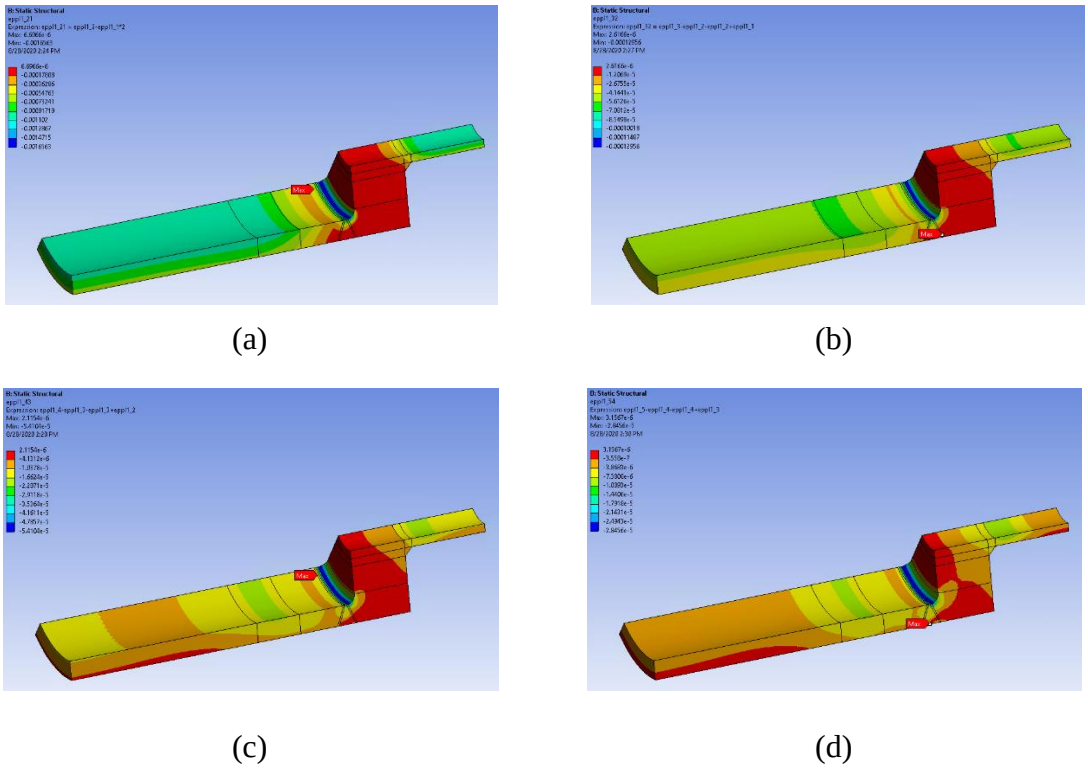

(a) (b)

(c) (d)

Figure 3.11. Difference of the ε_(p,total) changes. (a) 2nd cycle – 1st cycle, (b) 3rd cycle – 2nd cycle, (c) 4th cycle - 3rd cycle, (d) 5th cycle - 4th cycle.

Table 3.1. Max. ε (p,total) values and their increases at the end of each load cycle.

Cycle No.	$\varepsilon_{p,total}$	Change from previous cycle
1	2.1026E-3	2.103E-3
2	2.5583E-3	4.557E-4
3	2.8880E-3	3.297E-4
4	3.1637E-3	2.757E-4
5	3.4109E-3	2.472E-4

3.2.1.2.2 Maximum principal membrane strain and maximum principal surface strain checks

Figure 3.12 displays the strain linearization path in the endplate model. The maximum principal plastic membrane strain $\varepsilon_{p,m}$ was calculated along the path and point 1 and point 2 were inside wall and outside wall locations, respectively, for surface strain $\varepsilon_{p,m+b}$ calculations. The $\varepsilon_{p,m}$ and $\varepsilon_{p,m+b}$ strain linearization results are shown in Table 3.2; the magnitude differences from cycle to cycle for the first 5 load cycles are shown in Table 3.3. The data in Table 3.4 shows that the magnitude differences continue decreasing with additional cycles and the conservative estimations of $\varepsilon_{p,m}$ and $\varepsilon_{p,m+b}$ at the end of 30 cycles are equal to 7.70E-3 and 9.24E-3, respectively. These are lower than the 1% for membrane strain and 2% surface strain limits specified in HBB-T-1310.

As the strain linearization path was away from the weld, the full 1% and 2% membrane and bending limits were applied

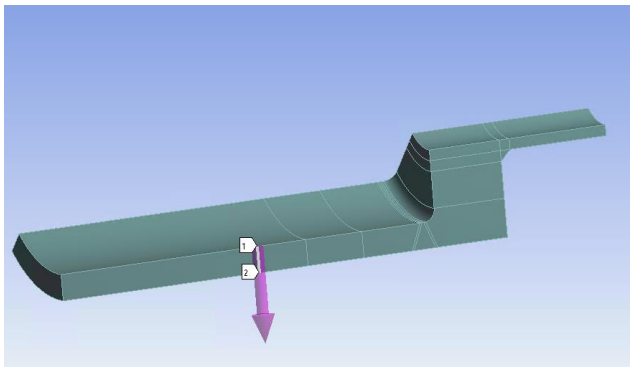

Figure 3.12. Strain linearization path for the endplate model.

Table 3.2. Results of inelastic strain linearization

Max.Principal Strain and Direction at the End of Each Cycle

Cycle No.	Membrane	Direction	Inside Wall	Direction	Outside Wall	Direction
1	1.146E-03	<0.697,0,-0.717>	1.411E-03	<0.697,0,-0.717>	8.805E-04	<0.697,0,-0.717>
2	1.417E-03	<0.697,0,-0.717>	1.741E-03	<0.697,0,-0.717>	1.093E-03	<0.697,0,-0.717>
3	1.650E-03	<0.697,0,-0.717>	2.023E-03	<0.697,0,-0.717>	1.277E-03	<0.697,0,-0.717>
4	1.876E-03	<0.697,0,-0.717>	2.293E-03	<0.697,0,-0.717>	1.458E-03	<0.697,0,-0.717>
5	2.100E-03	<0.697,0,-0.717>	2.560E-03	<0.697,0,-0.717>	1.640E-03	<0.697,0,-0.717>

Table 3.3. Maximum principal strain change differences.

Max.Principal Strain Changes from Previous Cycle

Cycle No.	Membrane	Inside Wall	Outside Wall
2	2.710E-04	3.300E-04	2.125E-04
3	2.330E-04	2.820E-04	1.840E-04
4	2.260E-04	2.700E-04	1.810E-04
5	2.240E-04	2.670E-04	1.820E-04

Table 3.4. Strain predictions at the end of the service life.

Max.Principal Strain Prediction

	Membrane	Inside Wall	Outside Wall
Values at the End of the 5th Cycle	2.100E-03	2.560E-03	1.640E-03
Max. Change during One Cycle	2.240E-04	2.670E-04	1.820E-04
At the End of the 30th Cycle	7.700E-03	9.235E-03	6.190E-03

3.2.2 Creep-fatigue

3.2.2.1 Core block

3.2.2.1.1 Creep damage

The creep damage was calculated based on the procedure described in Section 2.2.5. Creep damage over the first 5 cycles was explicitly calculated and the accumulation over the service life extrapolated from those results. Figure 3.13 (a) to (e) shows the creep damage results at the end of each

load cycle, the highest damages occurred at the webs between fuel rod holes and damage continues to increase cycle-to-cycle.

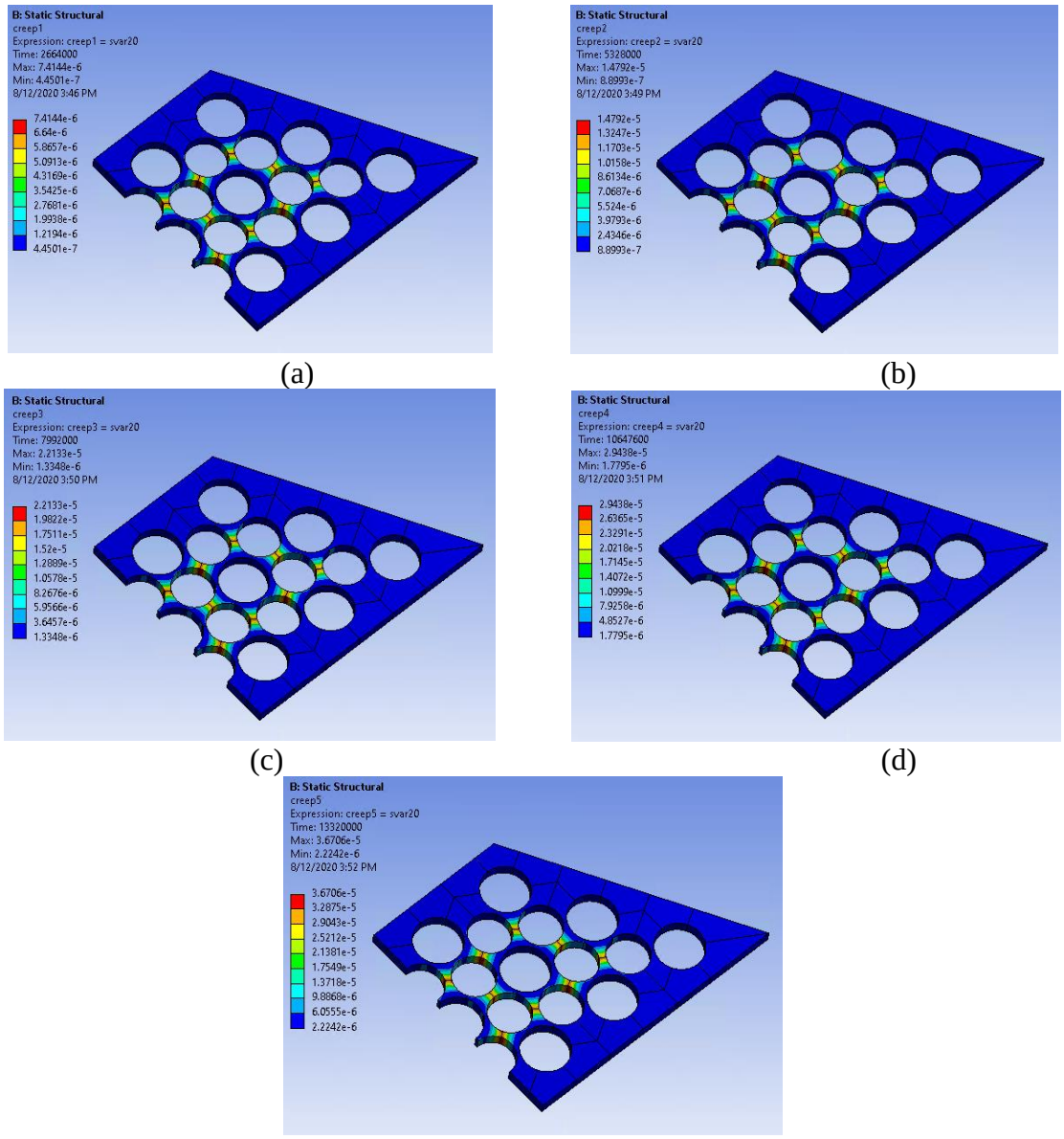

Figure 3.13. Creep damage at the ends of a load cycle. (a) 1st cycle. (b) 2nd cycle. (c) 3rd cycle. (d) 4th cycle. (e) 5th cycle.

Figure 3.14 (a) to (d) demonstrate the difference in creep damage increase magnitude from cycle to cycle. These plots show that the creep damage increases as time increase, but with decreasing magnitude, so, using the creep damage at the end of 5th cycle, shown in Figure 3.13 (e) and the creep damage increase during the 5th cycle, in Figure 3.14 (a), leads to a conservative estimation of creep damage at the end of 360th cycles (assumed load cycle number for the 30-year service life), displayed in Figure 3.15 (b). The maximum creep damage is 0.26%.

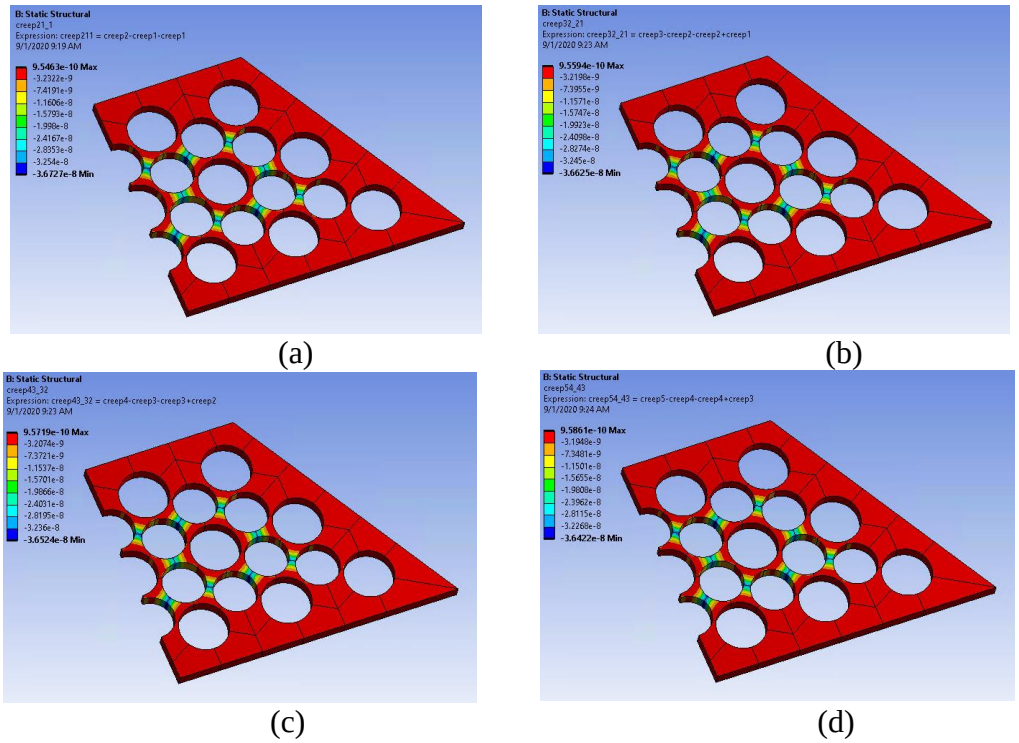

Figure 3.14. Difference of creep damage increase magnitudes between two consecutive cycles. (a) 2nd cycle – 1st cycle. (b) 3rd cycle – 2nd cycle. (c) 4th cycle – 3rd cycle. (d) 5th cycle – 4th cycle.

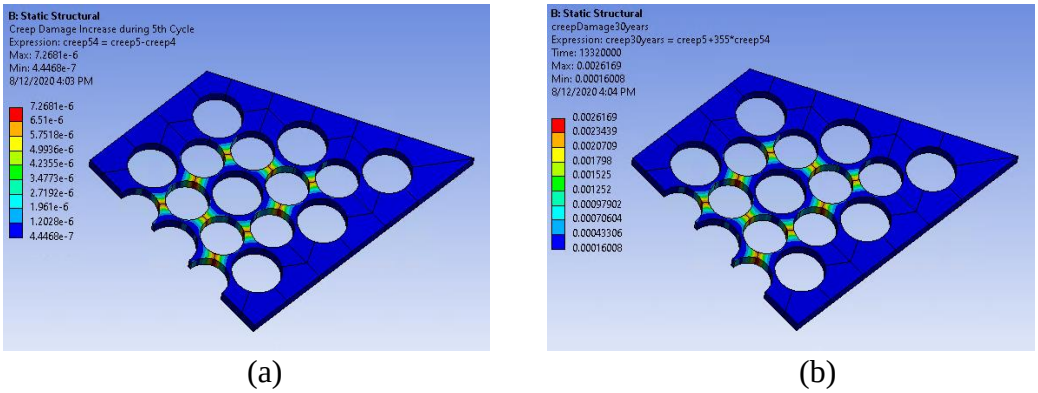

Figure 3.15. (a). Creep damage increase during the 5th cycle. (b) Creep damage at the end of 360th cycle.

These creep damage results were based on a K' factor of 0.67 obtained from Table HBB-T-1411-1 for inelastic analysis. Creep damage with a K' factor of 0.9, which is for elastic analysis, will be discussed in Chapter 3.2.2.2.1.

3.2.2.1.2 Fatigue damage

The core block structure operates in the elastic regime (inelastic strain in the order of 10^{-6}). Therefore, only the strain ranges for the first load cycle were calculated and can be conservatively applied to all load cycles. Figure 3.16 shows the strain range contour plot for the first load cycle. The highest strain range appeared in the web between fuel rod holes, and the maximum

strain range is equal to 8.2E-5. For Grade 91 material at 560°C, the allowable number of cycle is essentially infinity and the fatigue damage is 0.

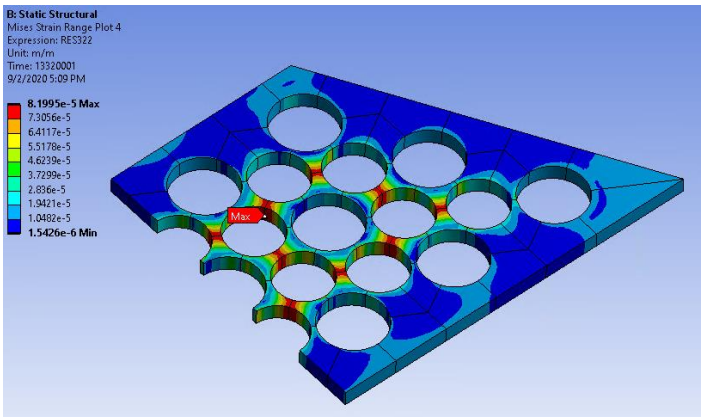

Figure 3.16. Equivalent strain range during the 1st load cycle.

3.2.2.1.3 Creep-fatigue interaction

The creep damage of the core block for 30-year service was about 0.26% and the fatigue damage was 0, so, based on the Code interaction diagram, the results fall within the envelope of the creep-fatigue damage and the component passes the design check.

3.2.2.2 Endplate

3.2.2.2.1 Creep damage

Figure 3.17 (a) to (e) shows the creep damage across the whole endplate model at the end of each load cycle. The highest creep damages are in the region near the welded joint, where the highest equivalent stress and highest plastic strain are located. Figure 3.17 (f) displays the creep damage contour plot after 13.7 days of service, when the value at the critical location of the model reached 1. Figure 3.18 (a) to (d) displays a decreasing trend for the creep damage magnitude changes from cycle to cycle. Therefore, we used the creep damage at the end of the 5th cycle together with the creep damage magnitude change during the 5th cycle to produce a conservative estimation of the creep damage at the end of the 30th cycle. These results are shown in Figure 3.19. The creep

damage is very high at the end of 30 years of service life, 12373%, far greater than 100%, the maximum allowable value per the Code rules.

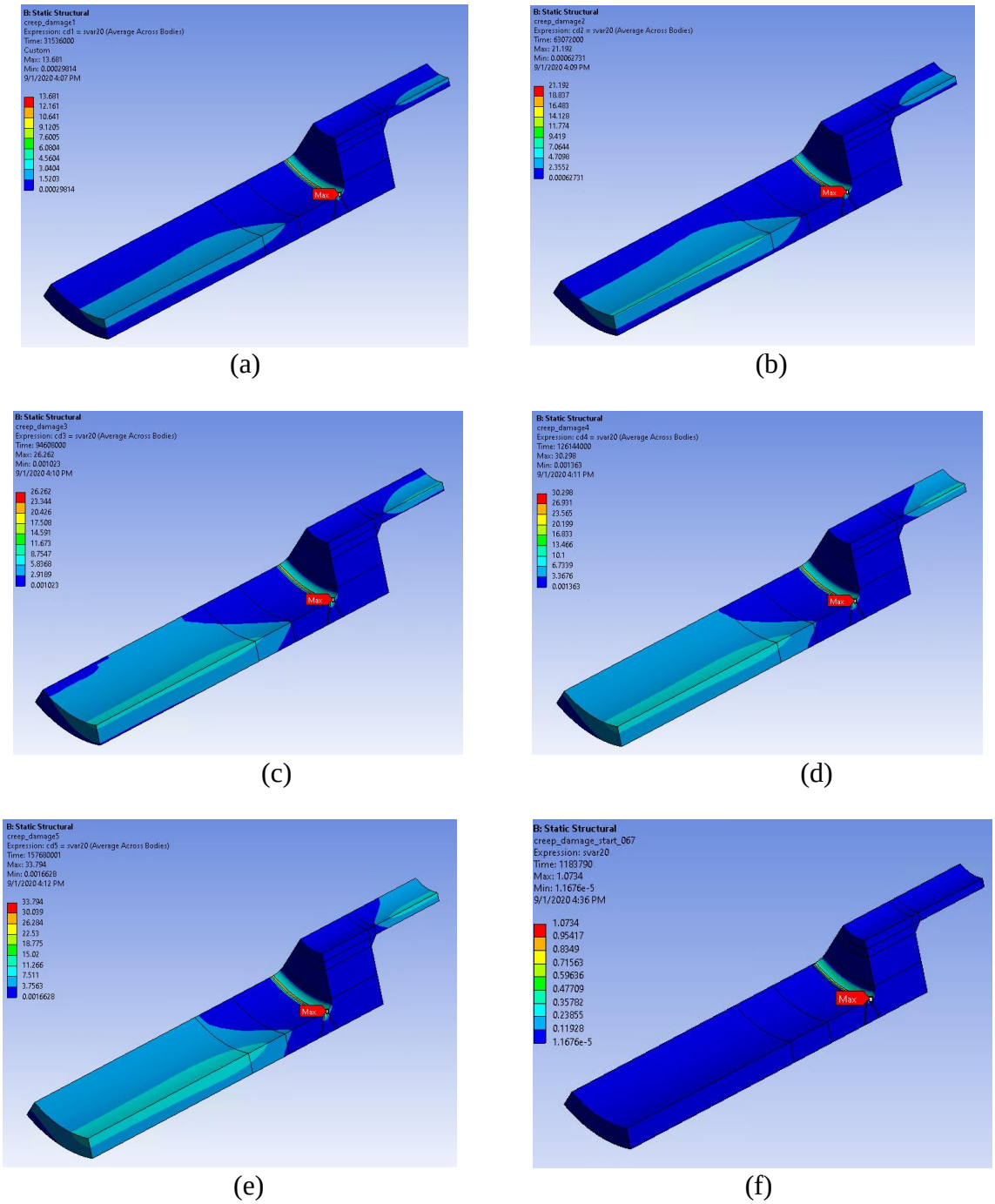

Figure 3.17. Creep life usage at the end of each load cycle of the endplate model (a) 1st cycle. (b) 2nd cycle. (c) 3rd cycle. (d) 4th cycle. (e) 5th cycle, and (f)13.7 days of service life.

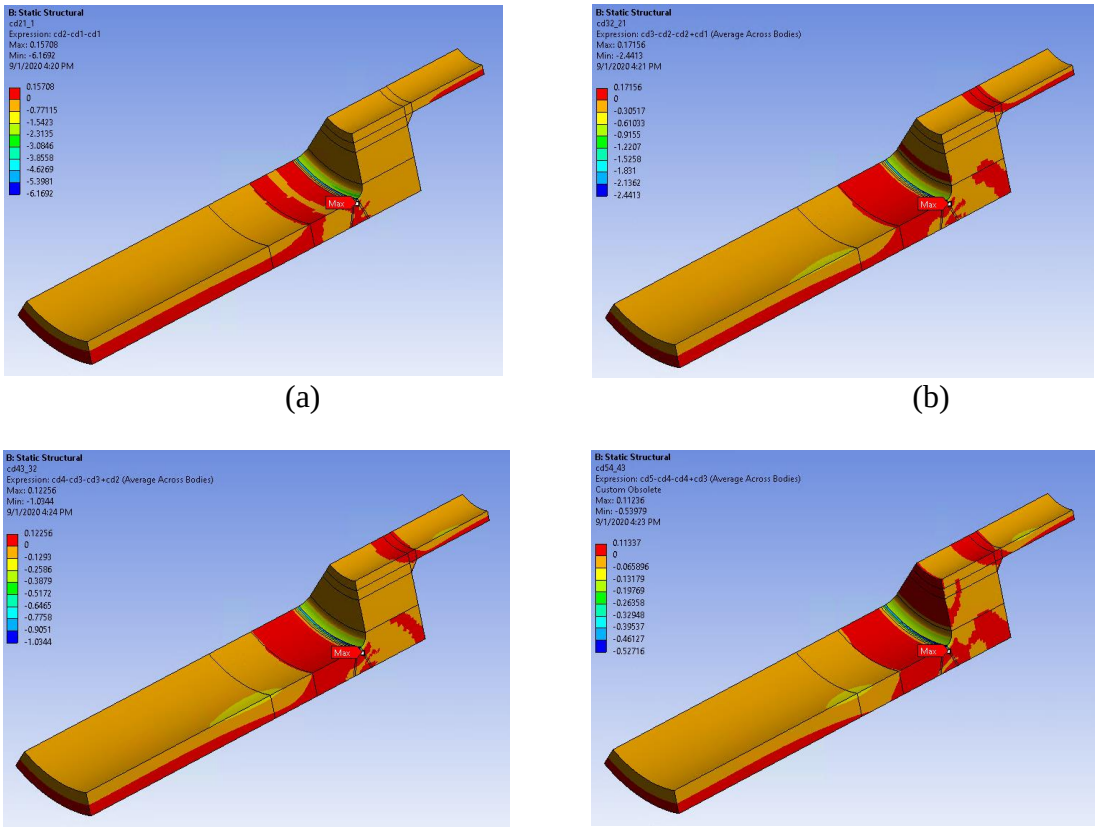

Figure 3.18. Creep damage increase magnitude differences from cycle to cycle for the endplate model. (a) 2nd cycle – 1st cycle. (b) 3rd cycle – 2nd cycle. (c) 4th cycle – 3rd cycle. (d) 4th cycle – 3rd cycle.

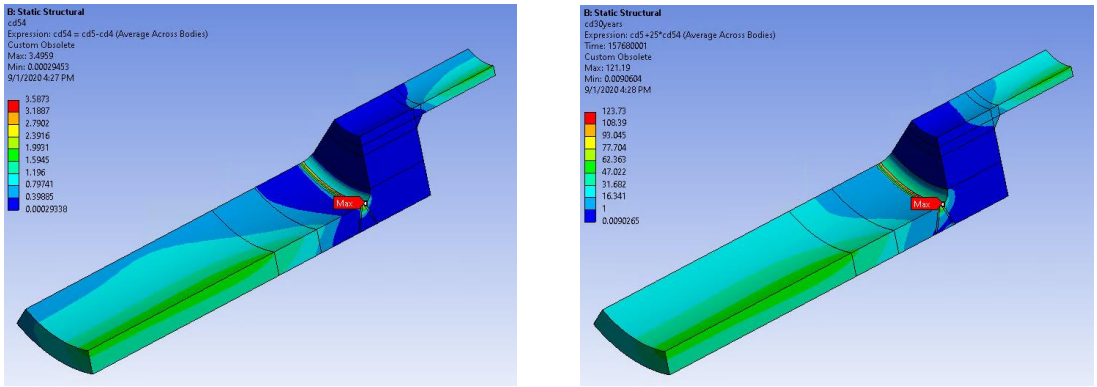

Figure 3.19. Creep damage prediction at the end of 30th cycle. (a) creep damage increase during 5th cycle. (b) Creep damage at the end of 30th cycle based on the data from (a) and Figure 3.17(e).

3.2.2.2.2 Fatigue damage

Figure 3.20 (a) to (e) plot the maximum strain range during each load cycle for the endplate model. The highest values always occur in the region close to the welded joint, and the values continue to decrease from cycle to cycle as shown in Table 3.5.

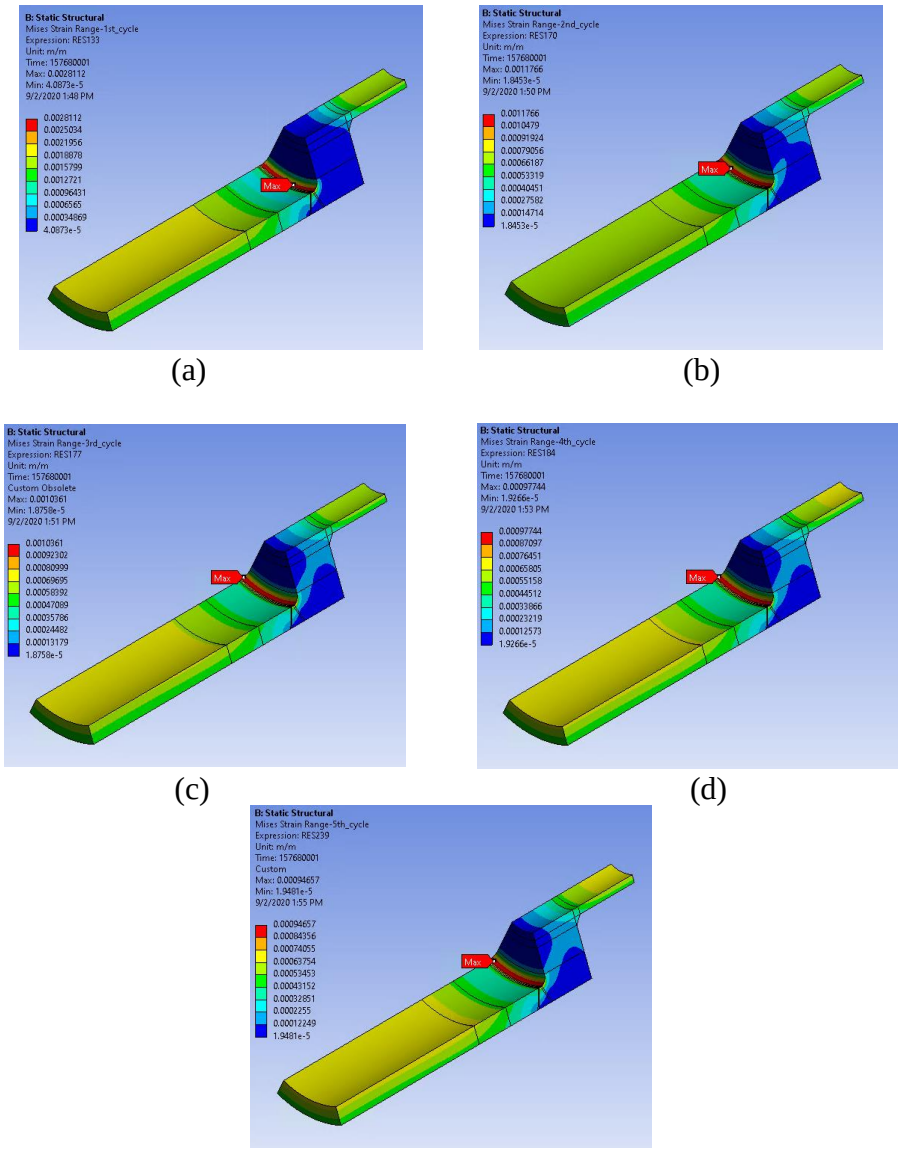

Figure 3.20. Maximum strain range during each load cycle. (a) 1st cycle. (b) 2nd cycle. (c) 3rd cycle. (d) 4th cycle. (e) 5th cycle.

Table 3.5. Highest strain range during each load cycle.

Cycle No.	Highest strain range (m/m)
1	2.81E-03
2	1.18E-03
3	1.04E-03
4	9.77E-04
5	9.47E-06

Probing the strain data at one of the high strain range locations shows the same trend shown in Table 3.5. Figure 3.21 plots the equivalent total strain at that location. The equivalent total strain

changes were calculated at the strain component level first, then based on those component values, the strain range changes were extrapolated.

With a strain range of 2.81E-3 and a temperature of 585° C, the allowable number of cycles is 5586 (0.5 factor for the weld was applied as the region is close to the welded joint), the fatigue damage for the required 30 cycles is 0.54%.

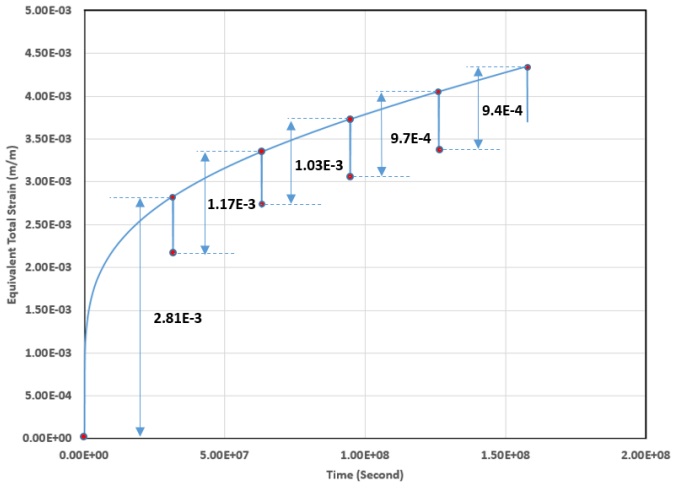

Figure 3.21. Equivalent total strain at the location with the highest strain range.

3.2.2.2.3 Creep-fatigue damage

While the fatigue damage for 30 cycles of a 30-year service life was less than 1%, the creep damage was very high for 30 year service life. Based on these results, we estimate the creep-fatigue life of the component as 14 days.

4 Discussion

4.1 Strain and deformation checks

4.1.1 Core block

As the pressure load is neglected and temperature ramping rate is 10 ^{o}C/hour, considering thermos-physical properties of Gr.91, thermal stress peaks are unlikely to occur during the ramp up/down. However, there are still some thermal stresses within the model due to inhomogeneous temperature distribution and constraints. But the maximum magnitude of equivalent stress is less than 18 MPa, as shown in Figure 4.1 (a), which is a contour plot of equivalent stress distribution, and Figure 4.1 (b), which shows the maximum equivalent stress within the whole component during the 5 load cycles. Figure 4.2 is the temperature distribution at full load condition. The maximum temperature is 559 ^{0}C. Considering that Grade 91's yield strength at 560° C is 256.8 MPa and a creep strain at 18MPa/560 ^{o}C for 30 years is about 0.2% [3], a simple calculation demonstrates that the magnitudes of inelastic strains should be small, much less than the inelastic strain limits specified in HBB-T-1310 of [1]. This simple calculation confirms the detailed design analysis discussed above.

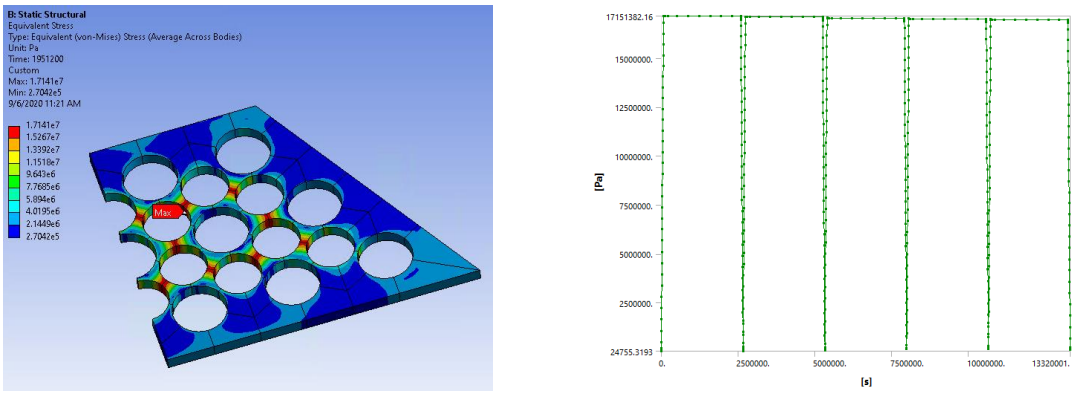

(a) (b)

Figure 4.1. (a) Equivalent stress during 1st cycle full load. (b). Maximum equivalent stress in each data frame during 5 load cycles.

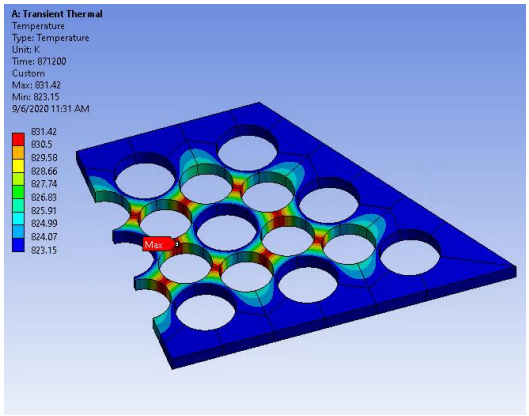

Figure 4.2. Temperature distribution during full load of the 1st load cycle.

4.1.2 Endplate

Figure 4.3 (a) shows the equivalent stress distribution at the beginning of the hold period of the 1st cycle. The maximum stress is around 130MPa at the location near the butt join. The location of maximum equivalent stress for other time steps are the same, but with different magnitudes. Figure 4.3 (b) plots the maximum equivalent stresses at that location for all time steps. It shows a maximum stress of 130MPa, which is reduced to about 75MPa, and then becomes stable. The maximum metal temperature at this location is 585° C. These conditions are much more severe than those for the core block problem, where the stress was 18MPa and the maximum metal temperature was 560° C. The strain and deformation checks confirm that the local maximum principal strain (0.96%), the maximum principal surface strain (0.92%) and maximum principal membrane strain (0.77%) are much higher than those for the core block.

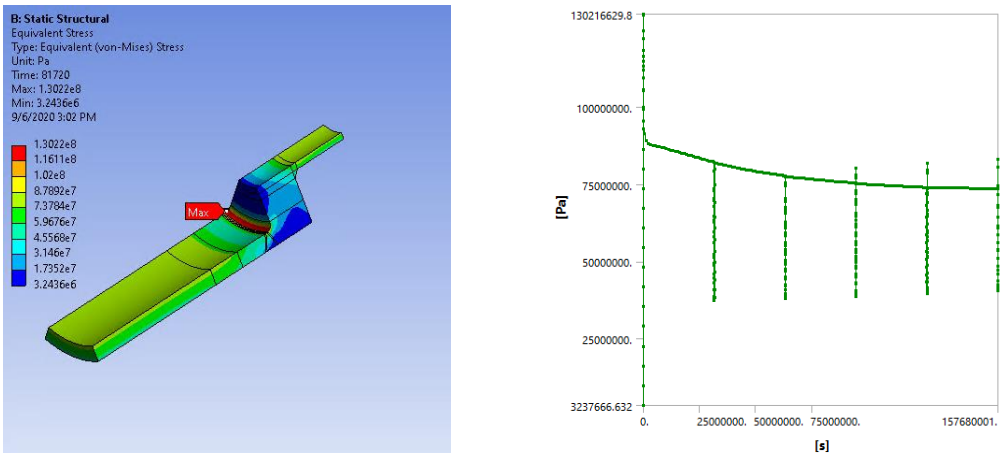

(a) (b)

Figure 4.3. Equivalent stress at the beginning of the full load holding for the 1st cycle. (b) maximum equivalent stress for 5 load cycles.

The strain linearization results also give the direction of the maximum inelastic membrane strain and that for the maximum inelastic surface (M+B) strain, they are along the hoop direction. Figure 4.4 displays the strain linearization path and the maximum strain direction.

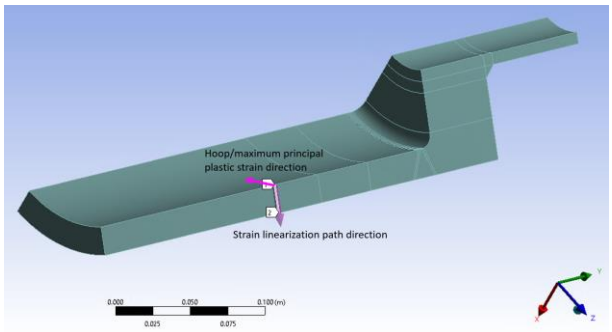

Figure 4.4. Strain linearization path and global coordinate system.

The results for the endplate are based on a mesh with 32,240 quadratic elements, which may need more refinement to verify result mesh-independency.

4.1.3 Design by inelastic analysis method compared to design by elastic analysis

Compared with elastic analysis, inelastic analysis does not need stress categorization, in other words, the stresses do not have to be put into categories due to primary load or secondary load. However, a strain linearization path (SLP) still has to be defined to calculate membrane strain and membrane plus bending strain. As strain categorization is unnecessary, for inelastic analysis, there is no need to run difference load cases during FEA, as for a design with elastic analysis.

4.2 Creep-fatigue check

4.2.1 Core block

Under the conditions of a full load temperature of 560^{o} C slow temperature ramping rates, and without a pressure load, the creep damage is low. The strain range is only 8.2E-5 during load cycles, which implies the structural remains elastic in the time-independent sense. Therefore, the material should be in high cycle fatigue (HCF) regime and the fatigue damage for 360 load cycles is negligible.

Even though the creep damage and fatigue damage are low for the expected service life of 30 years, the FEA results show a high creep damage zone and a high fatigue damage zone both located at the webs between fuel rod holes (shown in Figure 3.15 and Figure 3.16), which indicates locations that should be inspected for damage during outages.

To obtain the creep damage according to Equation 6 the effective stress was calculated. When $J_1/S_s\text{-}1 > 0$, the effective creep stress for damage calculation is larger than the von Mises stress, and when $J_1/S_s\text{-}1 <= 0$, the effective creep stress and von Mises equivalent stress are equal. Figure 4.5 shows the J_1/S_s-1 contour plot during the hold period for the 5th load cycle. This figure shows that the webs between fuel rod holes, where the highest creep-fatigue damage occurs, are in the $J_1/S_s\text{-}1 < 0$ regime. If this value was larger than 0 the effective creep stress would be larger than equivalent stress and creep-fatigue damage would be larger. This demonstrates how the current Code rules incorporate the 3D stress state into the creep damage calculation.

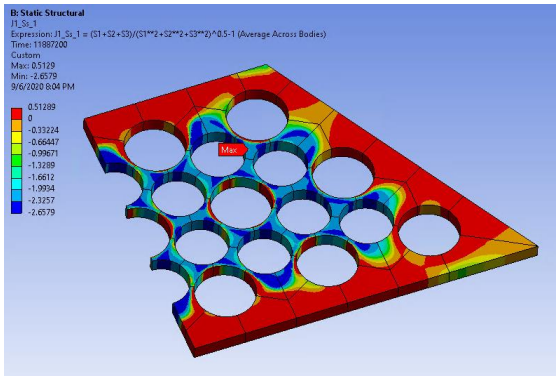

Figure 4.5. J_1/S_s-1 values across the core block.

4.2.2 Endplate

The highest creep damage occurs in the region close to the butt weld. A damage fraction of 1.0 occurs after about 14 days when applying a factor of *K'* = 0.67 as instructed in Table HBB-T-1411-1 of the Code. A *K'* factor of 0.9 was also considered, and the creep damage distribution is displayed in Figure 4.6. In this scenario100% creep damage occurs at one location after 379 days, that is a creep life more than 20 times longer than that by using a *K'* factor of 0.67. Potentially, the higher safety factor for design by inelastic analysis could be reduced to be in line with the 0.9 factor used in design by elastic analysis to produce less over conservative designs.

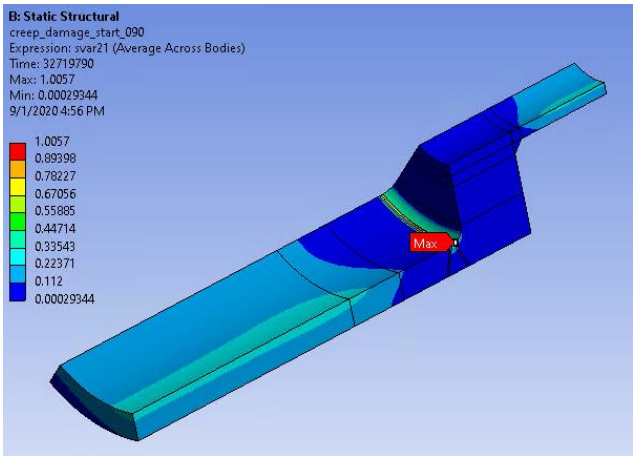

Figure 4.6. Creep damage distribution at the 379 days of service.

The highest fatigue damage zone occurs in the same zone the produces the highest creep damage, Table 3.5 shows the strain range decreases from cycle to cycle, and tends towards a constant value. This behavior reflects the process of the inelastic deformation zone in the region with the highest strain range becoming more and more stable, until finally the structure achieves plastic shakedown.

In the endplate model, both creep damage and fatigue damage are very localized, i.e., they are concentrated on a small region. The remainder of the structure undergoes significantly less creep-fatigue damage. This may indicate an inefficient design. Moreover, this suggests that an accurate fitness-for-service assessment of the component life would need to consider crack growth, not just the initiation of creep-fatigue damage.

4.2.3 Design by inelastic analysis method compared to design by elastic analysis

The creep-fatigue design procedure for design-by-inelastic analysis is much more straightforward than the procedure for design-by-elastic analysis. For example, the inelastic rules do not need results from different FEA load cases to calculate primary stress and secondary stress in order to get the *Z* factor to check for the requirements listed in HBB-T-1431 (a).(1) to (3). The design by inelastic analysis procedure is simple to execute, the challenge is getting appropriate stress analysis results using an inelastic constitutive model.

5 Conclusions

Inelastic analysis were conducted on a core block model and a endplate model by following ASME BPVC Section III, Division 5, Appendix HBB-T *Rules for strain, deformation, and fatigue limits at elevated temperatures*. In both models, creep damages are much higher than fatigue damages with the assumed pressure load and thermal load transients, and in each model, the highest creep damage and the highest fatigue damage occur in the same region. There are several advantages of the design by inelastic analysis rules, compared to design by elastic analysis:

- The inelastic analysis rules are easier to follow and the results are straight forward to interpret.
- Stress categorization is unnecessary and complicated calculation procedures for addressing creep and plasticity in the elastic procedures are unnecessary.

No significant challenges were noted in executing the current Code rules using the ANL constitutive model. The model produces a reasonable response for Grade 91 over the stress and temperature conditions sampled in the design analyses.

However, there are aspects of the inelastic rules that could benefit from additional exploration as part of future code development efforts:

- The dependence of the inelastic stress analysis results on the time step size, i.e. time integration error, could lead to inaccuracy. This is not an issue with elastic stress analysis.
- Mesh sensitivity. This issue was only partly addressed in these sample problems. A complete design analysis would need to include a mesh sensitivity study. Mesh sensitivity will be more of an issue for design by inelastic analysis because the stress linearization procedure applied in design by elastic analysis tends to reduce the effects of mesh sensitivity.
- The strain linearization procedure in the design by inelastic analysis rules. This is the last remnant of the classical ASME linearization process. Replacing this part of the strain limits criteria by some criteria at FE integration point would greatly simplify the design by inelastic analysis rules as they could be fully automated, for example using the ANSYS scripting capability.
- The difference between the 0.9 factor applied to the effective stress in the design by elastic analysis creep damage procedure versus the 0.67 factor specified for design by inelastic analysis. This factor significantly penalizes the inelastic method as rupture times tend to follow a power law relation with stress at fixed temperature. The origins of this difference between the two methods should be explored and, if possible, the safety factor in the design by inelastic analysis check reduced to reduce over conservatism and avoid unduly penalizing the more exact inelastic method.
- For both sample problems, fully simulating the entire component load history is infeasible. While modern computers can handle much larger simulations in terms of the component volume or number of elements in the discretization through parallel computing, time integration cannot be parallelized. Therefore, if the design specification includes a large number of individual transients or a large number of transient repetitions, the resulting full inelastic analysis will be computationally expensive. As in this report, this challenge can

be partly addressed by extrapolating strain and damage accumulation from a smaller number of simulated load cycles. However, additional research and development should address the general problem of time integration for inelastic analysis, in order to make the processes easier for component vendors and designers.

These suggestions would optimize the current inelastic analysis Code rules. The sample problems here demonstrate the current rules are adequate and can be applied to a wide variety of representative component geometries and loadings.

ACKNOWLEDGEMENTS

This research was sponsored by the U.S. Department of Energy, under Contract No. DEAC0206CH11357 with Argonne National Laboratory, managed and operated by UChicago Argonne LLC. Programmatic direction was provided by the Office of Nuclear Reactor Deployment of the Office of Nuclear Energy. The authors gratefully acknowledge the support provided by Sue Lesica, Federal Manager, Advanced Materials, Advanced Reactor Technologies (ART) Program, Tom Sowinski, Federal Manager, Microreactor Program, and Jess C. Gehin of Idaho National Laboratory, National Technical Director, Microreactor Program.

REFERENCES

[1] *ASME Boiler and Pressure Vessel Code 2019*, Section III, Division 5, American Society of Mechanical Engineers, Little Falls, NJ, 2019.

[2] Messner, M.C, Phan, V.-T. and Sham, T.-L. *A Unified Inelastic Constitutive Model for the Average Engineering Response of Grade 91 Steel*, p1–10, Proceedings of ASME 2018 Pressure Vessels and Piping conference, PVP2018, July 15-20, 2018, Prague, Czech Republic.

[3] *hbbdata Documentation, Release 0.1,* Argonne National Laboratory, August 2019.

[4] *Recommended Practices in Elevated Temperature Design: A Compendium of Breeder Reactor Experiences (1970-1987) Volume III – Inelastic Analysis.* Dhalla, A. K., ed. Welding Research Council Bulletin, 1991.

[5] D. Dewees et al. "Comparison of Candidate Steady Loading Elevated Temperature Design-by-Analysis Methods." In the *Proceedings of the ASME 2020 Pressure Vessels & Piping Conference*, PVP2020-21573, 2020.

Applied Materials Division
Argonne National Laboratory
9700 South Cass Avenue, Bldg. 212
Argonne, IL 60439

www.anl.gov